GEOPHYSICS, VOL. 49, NO. 8 (AUGUST 1984); P. 1180–1187, 6 FIGS., 2 TABLES.

The Radon transform and its properties

T. S. Durrani* and D. Bisset*

ABSTRACT

This paper presents a summary of the fundamental properties of the Radon transform, including delay effects, data shifting, rotation, scaling, windowing, bowtie events, energy conservation, etc., and includes representative examples on standard data sets such as 2-D delta functions, boxcar events, Gaussian bell, and conic sections which reinforce the basic concepts of the Radon transform.

INTRODUCTION

New techniques for the solution of inverse problems in signal processing are gaining increasing interest. Such problems arise when a requirement exists for imaging a complete field of view from data collected at fixed locations. Applications occur in a number of areas, such as seismic signal processing, for determining the constituents of the earth from observations taken at the earth's surface; in radiography, ultrasonic, or x-rays, (Shepp and Logan, 1974), as in tomography for the estimation of attenuation parameters from projection data (Boerner et al., 1981); in remote sensing; and in system identification from output data only. To attack such problems, the Radon transform and its inverse are finding renewed use (Robinson, 1982; Chapman, 1981).

The two-dimensional (2-D) Radon transform (Gelfand, 1966) is a mapping of 2-D data defined over a rectangular set of coordinates (x, y) onto a domain defined by the slope and intercept (p, τ) of lines present in the data. This allows line integrals in the (x, y) domain to be mapped into points in the (p, τ) domain. The inverse transform performs the inverse mapping of generating ray paths (lines) from points in the (p, τ) domain.

DEFINITION

Robinson (1982) defines the Radon transform as

$$R_{p\tau}\{f(x, y)\} = \int_{-\infty}^{\infty} f(x, \tau + px)\, dx, \tag{1}$$

where $f(x, y)$ depicts a 2-D function in R^2 domain $(\forall x, y)$ and where the y coordinate of $f(x, y)$ occurs on the line $y = \tau + px$ in x-y space.

Using the sampling property of the delta function, the above equation may be recast as the double integral

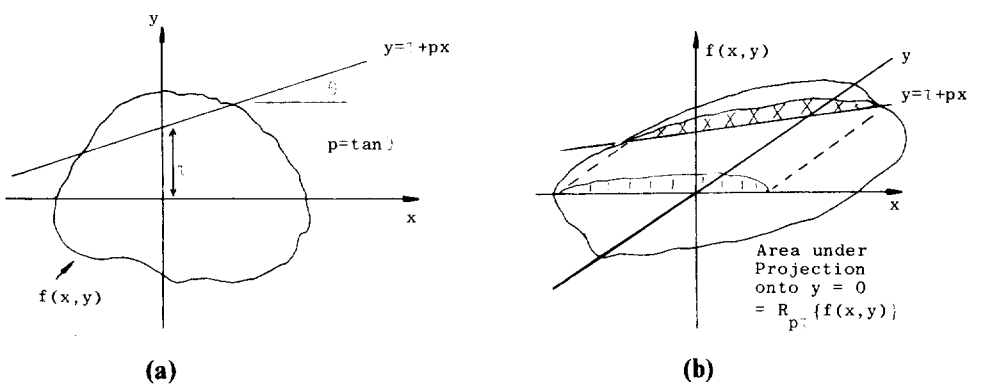

FIG. 1. Integration of an object along the line $y = \tau + px$. (b) is an isometric view of (a).

Manuscript received by the Editor August 10, 1983; revised manuscript received February 6, 1984.
*Dept. of Electronic and Electrical Engineering, University of Strathclyde, 204 George Street, Glasgow G1 1XW, United Kingdom.

$$R_{p\tau}\{f(x, y)\} = \int_{-\infty}^{\infty}\int_{-\infty}^{\infty} f(x, y)\delta[y - (\tau + px)]\, dy\, dx. \quad (2)$$

From equations (1) and (2), a symbolic definition for the Radon transform may be given as

$$R_{p\tau}\{f(x, y)\} \triangleq U(p, \tau). \quad (3)$$

The area under the cross-hatched region in Figure 1b represents the line integral (L.I.$_{p\tau}$) for the slope p and intercept τ. The integral of equation (1), $R_{p\tau}\{f(x, y)\}$, is the area of the projection onto $y = 0$ of the cross-hatched area.

The plot of the Radon transform is a map of the integral with reference to x along lines with chosen slope (p) and intercept (τ) onto a plane with coordinates p (for slope) and τ (for intercept). To obtain the complete Radon transform of a function, the integral, equation (1), is performed for the range $p = -\infty$ to $+\infty$ and for $\tau = -\infty$ to $+\infty$ with corresponding values of equation (1) for each p and τ value being plotted in the p-τ plane.

For example, a function which frequently arises in 2-D data is the boxcar which depicts a 2-D window in the x-y domain. The Radon transform for this function is shown as the second transform pair in Table 2.

PROPERTIES OF THE RADON TRANSFORM

Table 1 lists various properties of the Radon transform. The proofs of these properties follow directly from the basic definition. However, the proof of the skewing is included here to illustrate the development of the related proofs, i.e.,

$$R_{p\tau}\{f(a_1x + b_1y, a_2x + b_2y)\} = \frac{1}{|a_1 + b_1p|}\, U\left\{\frac{a_2 + b_2p}{a_1 + b_1p}, \frac{\tau[a_2 - b_1(a_2 + b_1b_2)]}{a_1 + b_1p}\right\}.$$

Figures 2a and 2b show the plan of a 2-D boxcar and a 2-D skewed boxcar to illustrate the effect of skewing on a function.

Proof From equation (2) we have

$$R_{p\tau}\{f(a_1x + b_1y, a_2x + b_2y)\} = \int_{-\infty}^{\infty}\int_{-\infty}^{\infty} f(a_1x + b_1y, a_2x + b_2y)\delta[y - (\tau + px)]\, dy\, dx$$

$$= \int_{-\infty}^{\infty} f[x(a_1 + b_1p) + b_1\tau, x(a_2 + b_2p) + b_2\tau]\, dx.$$

Letting

Table 1. Properties of the Radon transform.

Theorem	Function	Radon transform
Definition	$f(x, y)$	$R_{p\tau}\{f(x, y)\} = \int_{-\infty}^{\infty} f(x, \tau + px)\, dx \equiv U(p, \tau)$
Superposition	$f_1(x, y) + f_2(x, y)$	$U_1(p, \tau) + U_2(p, \tau)$
Linearity	$af(x, y)$	$aU(p, \tau)$
Scaling	$f\left(\frac{x}{a}, \frac{y}{b}\right)$	$\lvert a\rvert U\left(p\frac{a}{b}, \frac{\tau}{b}\right)$
Delay	$f(x - a, y - b)$	$U(p, \tau - b + pa)$
Rotation	$f(x, y)/\underline{\phi}$	$\frac{1}{\lvert\cos\phi + p\sin\phi\rvert}\, U\left(\frac{p - \tan\phi}{1 + p\tan\phi}, \frac{\tau}{\cos\phi + p\sin\phi}\right)$
Skewing	$f(ax + by, cx + dy)$	$\frac{1}{\lvert a + bp\rvert}\, U\left\{\frac{c + dp}{a + bp}, \tau\frac{[d - b(c + bd]}{a + bp}\right\}$
Relationship to line integral (L.I.)		L.I.$_{p\tau} = \sqrt{1 + p^2}\, U(p, \tau)$
Projection slice (1)		$\int_{-\infty}^{\infty} U(p, \tau)e^{-j\Omega\tau}\, d\tau = F(-\Omega p, \Omega)$ (2-D Fourier transform)
Projection slice (2)		$\frac{1}{2\pi}\int_{-\infty}^{\infty} R_{p\tau}\{F(\omega_1, \omega_2)\}e^{j\Omega\tau}\, d\tau = 2\pi f(-\Omega p, \Omega)$
1-D convolution theorem		$R_{p\tau}\{f(x, y) * g(y)\} = U(p, \tau) * g(\tau)$
Plancheral's theorem		$\int_{-\infty}^{\infty} U(p, \tau)\, d\tau = \int_{-\infty}^{\infty}\int_{-\infty}^{\infty} f(x, y)\, dx\, dy$
Parseval's theorem		$\int_{-\infty}^{\infty} R_{p\tau}\{f^2(x, y)\}\, d\tau = \int_{-\infty}^{\infty}\int_{-\infty}^{\infty} f^2(x, y)\, dx\, dy$

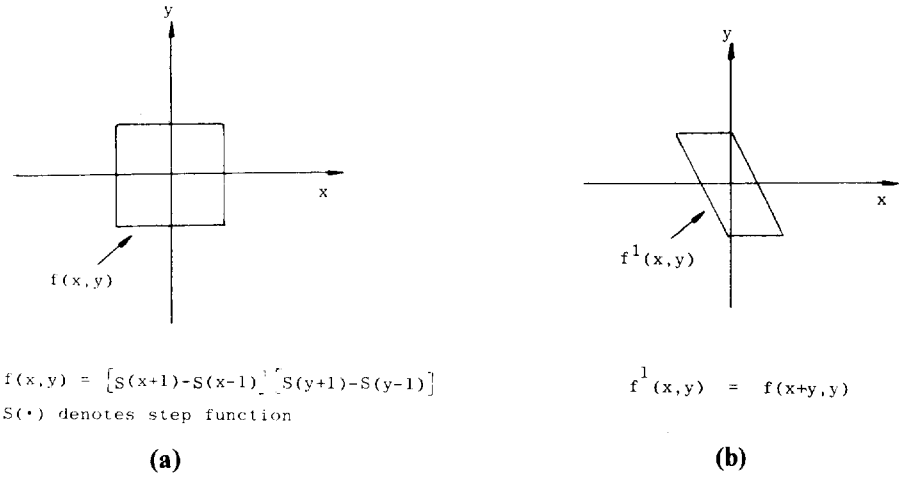

FIG. 2. Plan of a boxcar function. (b) shows the plan of the skewed version of the boxcar.

$$u = x(a_1 + b_1 p) + b_1 \tau$$

and therefore

$$dx = \frac{du}{|a_1 + b_1 p|},$$

leads to

$$R_{p\tau}\{f(a_1 x + b_1 y, a_2 x + b_2 y)\} = \frac{1}{|a_1 + b_1 p|} U\left\{\frac{a_2 + b_2 p}{a_1 + b_1 p}, \frac{\tau[a_2 - b_1(a_2 + b_1 b_2)]}{a_1 + b_1 p}\right\}.$$

The rotation theorem is a special case of the skewing theorem, the relevant geometry of which is shown in Figure 3.

The second section of Table 1 lists various theorems of the Radon transform. The first is the well-known projection slice theorem (1) which states that the (1-D) Fourier transform of the Radon transform yields the 2-D Fourier transform along a line (slice) in the 2-D frequency plane. The projection slice theorem (2) states the inverse proposition to the above. This may be proved by considering the function $f(x, y)$ as the 2-D inverse Fourier transform which yields

$$f(x, y) = \frac{1}{4\pi^2} \int_{-\infty}^{\infty} \int_{-\infty}^{\infty} F(\omega_1, \omega_2) e^{j\omega_1 x} e^{j\omega_2 y}\, d\omega_1\, d\omega_2,$$

and

$$f(-py, y) = \frac{1}{4\pi^2} \int_{-\infty}^{\infty} \int_{-\infty}^{\infty} F(\omega_1, \omega_2) e^{-j\omega_1 py} e^{j\omega_2 y}\, d\omega_1, d\omega_2.$$

Letting

$$\omega_2 = \tau + p\omega_1,$$

and

$$\omega_1 = \omega_1.$$

Since the Jacobian of the transformation is unity, we obtain

$$f(-py, y) = \frac{1}{4\pi^2} \int_{-\infty}^{\infty} \int_{-\infty}^{\infty} F(\omega_1, \tau + p\omega_1) \cdot e^{-j\omega_1 py} e^{jy(\tau + p\omega_1)}\, d\omega_1\, d\tau,$$

and

$$2\pi f(-py, y) = \frac{1}{2\pi} \int_{-\infty}^{\infty} \left\{ \int_{-\infty}^{\infty} F(\omega_1, \tau + p\omega_1)\, d\omega_1 \right\} e^{jy\tau}\, d\tau.$$

The right-hand side of this expression can be recognized as the 1-D inverse Fourier transform of the term within the braces. This term is itself the Radon transform of $F(.,.)$, where $F(.,.)$ is the 2-D Fourier transform of the function $f(x, y)$. Thus this theorem implies that the 1-D inverse Fourier transform of a Radon transformed 2-D frequency function $F(.,.)$ is equal to a slice of the equivalent spatial function $f(x, y)$.

The 1-D convolution theorem states that the Radon transform of the convolution of a 2-D function with a 1-D function (of y) is equal to the 1-D convolution (of the Radon transformed value) of the 2-D function with the same 1-D function, after an appropriate change of axis (y replaced by τ).

The last two entries in Table 1 summarize the energy conservation properties in the x-y and p-τ domains, respectively.

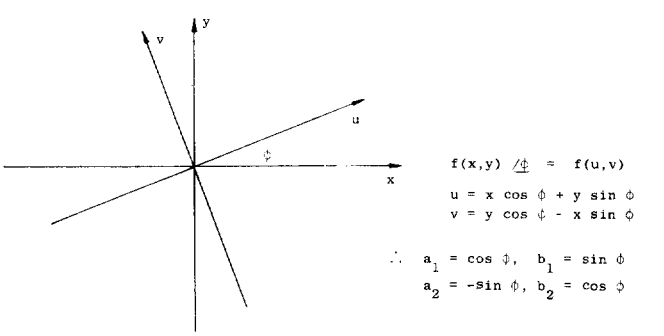

FIG. 3. Transformation of coordinates due to rotation.

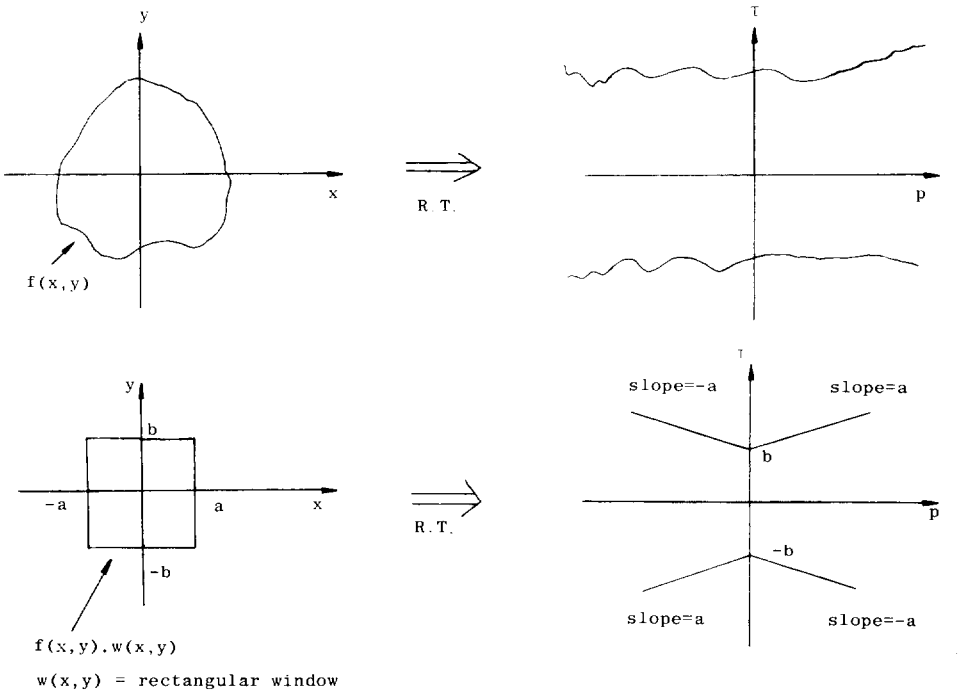

FIG. 4. Regions of support in the x-y and p-τ domains for a function and its rectangular window truncated function.

WINDOWING EFFECTS

Two-dimensional data, defined over a finite support, may be considered as truncated by multiplying the 2-D field by a boxcar, as shown in Figure 4. The effect of multiplying a 2-D function by the rectangular boxcar is to confine the range of values for the Radon transform to lie within a bowtie. The parameters of the bowtie may be evaluated by considering the vertices of the 2-D boxcar and the sixth transform pair shown in Table 2.

Considering the point located at $x = a$, $y = b$ as a delta function $\delta(x - a)\delta(y - b)$, whose Radon transform is $\delta[b - (\tau + pa)]$, the point (a, b) thus maps into the line $\tau = b - pa$ and therefore defines one of the boundaries for the values of the Radon transform. This procedure may be performed on the three other vertices of the boxcar to evaluate the remaining boundaries of the Radon transform.

The values of the Radon transform within the bowtie are less than that for the Radon transform of the untruncated function. This is due to the limits of integration extending only to the

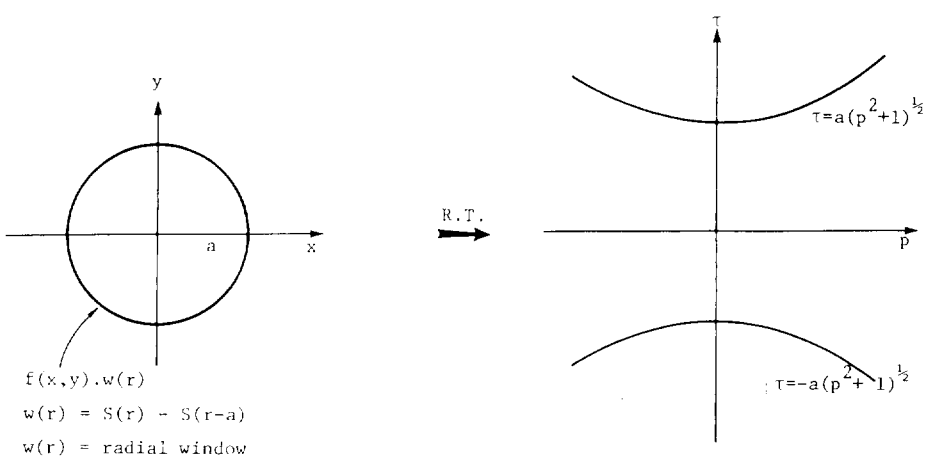

FIG. 5. Region of support in the x-y and p-τ domains for a function truncated by a radial window of radius a.

Table 2. Representative examples.

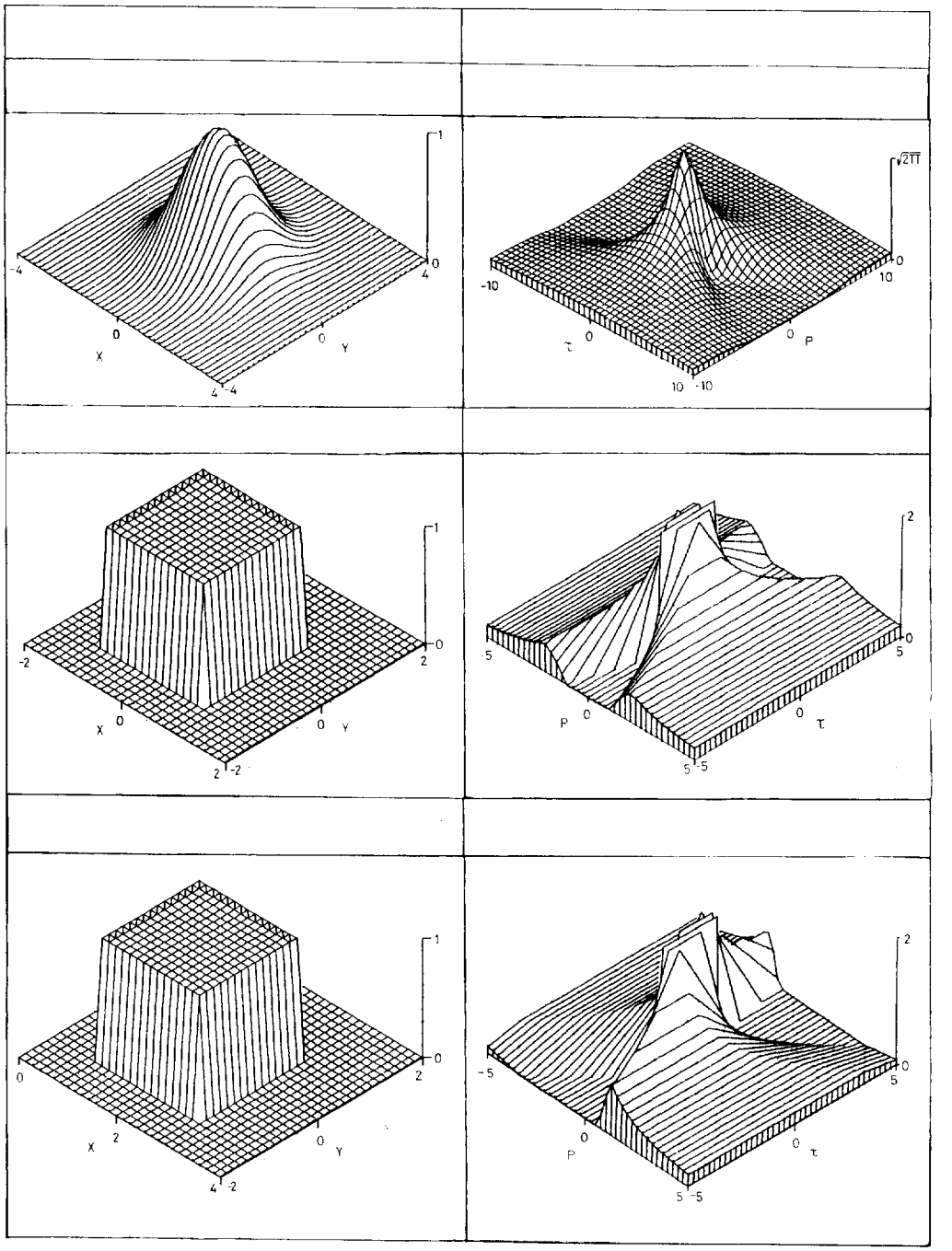

Table 2. continued. Representative examples.

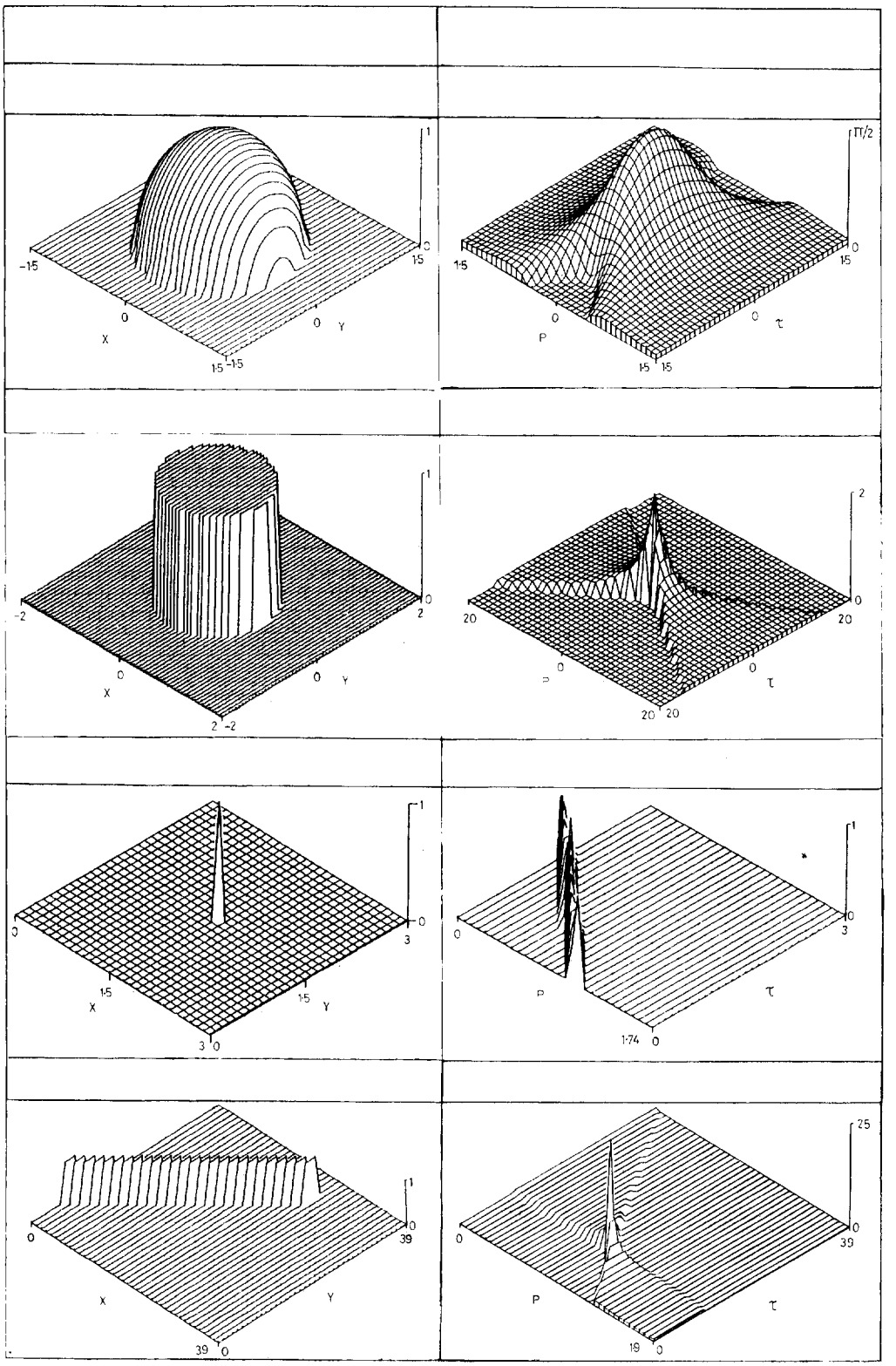

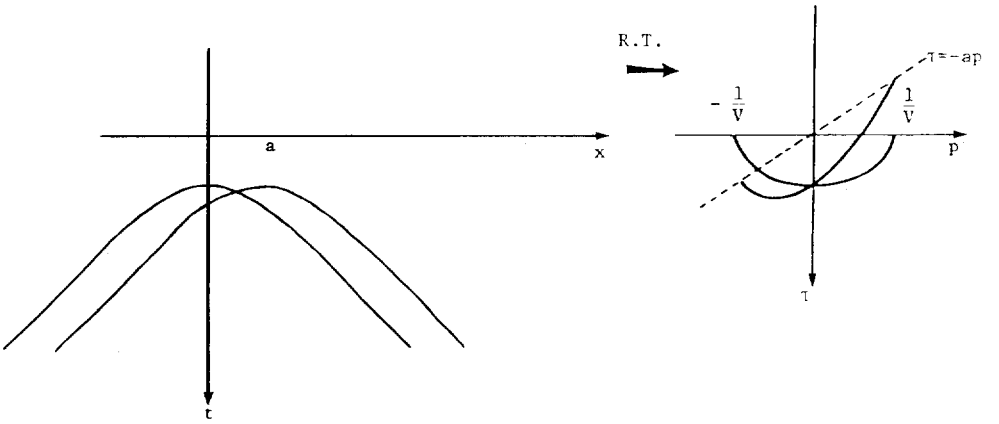

FIG. 6. Two time-distance hyperbolas and their slant stacks. The hyperbola $t = 1/v\sqrt{x^2 + h^2}$ transforms to the ellipse $\tau = h\sqrt{v^{-2} - p^2}$, whereas the hyperbola $t = 1/v\sqrt{(x-a)^2 + h^2}$ transforms to the ellipse $\tau = h\sqrt{v^{-2} - p^2} - pa$.

boundary of the boxcar and not from $-\infty$ to $+\infty$; hence windowing in the space domain manifests itself as a bowtie effect in the p-τ domain.

Truncating a function by the use of a cylinder creates a hyperbolic shaped bowtie on the p-τ plane. This is shown in Figure 5.

The bowtie boundary may be evaluated by considering the boundary of the truncated function

$$y = \pm(a^2 - x^2)^{1/2},$$

and

$$p = \frac{dy}{dx} = \mp x(a^2 - x^2)^{-1/2},$$

hence

$$x = \pm ap(p^2 + 1)^{-1/2}.$$

However, since

$$y = \tau + px,$$

we obtain a value of τ as

$$\tau = \pm x(p^2 + 1)/p.$$

Substituting for x and squaring, we obtain

$$\tau^2 = a^2(p^2 + 1). \tag{4}$$

This is a hyperbola in (p, τ) space.

Equation (4) therefore defines the range of values in the p-τ domain for the Radon transform of a cylindrically truncated function.

INVERSE RADON TRANSFORM

This paper has concentrated on the presentation of the Radon transform for a general 2-D data field. An inverse Radon transform operator exists (Robinson, 1982) which is given by

$$f(x, y) = \frac{1}{2\pi}\int_{-\infty}^{\infty} \frac{d}{dy} H\{U(p, y - px)\}\, dp,$$

where $H\{\cdot\}$ = Hilbert transform operator.

The convolution operation of $(d/dy)H\{.\}$ is equivalent to the multiplication operation of a symmetric ramp $|\omega|$ in the frequency domain; consequently this type of inverse Radon transform operation is called an $|\omega|$ – filtered back projection. Various convolution operators, which are variants on $|\omega|$, have been proposed (Kwoh et al., 1977) with a view to yielding improved reconstructions. The projection slice theorem also provides a method for obtaining the inverse Radon transform (Taylor, 1967) via the 2-D inverse Fourier transform.

DISCUSSION

While Table 1 lists various properties of the 2-D Radon transform, Table 2 gives expressions and illustrations for a number of currently used functions in the space domain. The first example shows the Radon transform pair for a Gaussian bell. This provides a good analytical example for verification of the projection slice theorem.

The second example shows the Radon transform pair for a 2-D boxcar, while the third example shows the Radon transform pair for the horizontally delayed boxcar.

An interesting example of the delay theorem could arise in the case of a stacked section consisting of the waveforms due to two point diffractors in a homogeneous medium, both at the same depth but with one diffractor situated at $x = 0$ and the other at $x = a$. Both point diffractors will give rise to diffraction hyperbolas which upon slant stacking (which is the geophysical equivalent of the Radon transform) will result in ellipses. The slant stack of the hyperbola situated at $x = 0$ will be the familiar ellipse, but the slant stack of the hyperbola with its apex occurring at $x = a$ will yield a skewed ellipse. This is shown in Figure 6. The ellipses intersect each other only on the τ-axis, and the value of τ for the skewed ellipse cannot be regarded as the usual meaning of τ (the sum of the vertical slowness-thickness products), although it is closely related to it.

The last two examples in Table 2 show the Radon transform pairs of points and lines, respectively. These examples illustrate the well-known result that points transform to lines and that lines transform to points. The last example depicts an approximate delta line because it has finite thickness. As a result, low-amplitude values fall within the bowtie region. This phenomenon has been termed aliased energy (Schultz and Claerbout, 1978), and Stoffa et al. (1981) have proposed a method to reduce this using semblance.

Applications of the Radon transform have been well documented in tomography and in seismic signal processing such as the separation of reflections, refractions, and ground roll (Tatham et al., 1982), coherent noise reduction (Noponen and Keeney, 1983), and inversion of common midpoint data (Diebold and Stoffa, 1981). It is envisaged that the set of results presented here will lead to more informed use of the Radon transform.

REFERENCES

Boerner, W. M., Jordan, A. K., and Kay, I. W., 1981, Introduction to the special issue on inverse methods in electromagnetics: Trans. Inst. Electr. and Electron. Eng., **AP-29**, 185–190.

Chapman, C. H., 1981, Generalized Radon transforms and slant stacks: Geophys. J. Roy. Astr. Soc., **66**, 445–453.

Diebold, J. B., and Stoffa, P. L., 1981, The traveltime equation, tau-p mapping inversion of common midpoint data: Geophysics, **46**, 238–254.

Gelfand, I. M., 1966, Generalized functions: **5**, Academic Press, Inc.

Kwoh, Y. S., Reed, J. S., and Truong, T. K., 1977, A generalized $|\omega|$-filter for 3-D reconstruction: Trans. Inst. Electr. and Electron. Eng., **NS-21**, 1990–1995.

Noponen, I., and Keeney, J., 1983, Attenuation of waterborne coherent noise by application of hyperbolic velocity filtering during the tau-p transform: Presented at the 53rd Annual International SEG Meeting, September 12, in Las Vegas.

Robinson, E. A., 1982, Spectral approach to geophysical inversion by Lorentz, Fourier and Radon transforms: Proc. Inst. Electr. and Electron. Eng., **70**, 1039–1053.

Shepp, L. A., and Logan, B. F., 1974, The Fourier reconstruction of a head section: Trans. Inst. Electr. and Electron. Eng., **NS-21**, 21–44.

Schultz, P. S., and Claerbout, J. F., 1978, Velocity estimation and downward continuation by wavefront synthesis: Geophysics, **43**, 691–714.

Stoffa, P. L., Buhl, P., Diebold, J. B., and Wenzel, F., 1981, Direct mapping of seismic data to the domain of intercept time and ray parameter—A plane-wave decomposition: Geophysics, **46**, 255–267.

Tatham, R. H., Keeney, J. W., and Noponen, I., 1982, Application of the tau-p transform (slant stack) in processing seismic reflection data: Presented at the 52nd Annual International SEG Meeting October 19, 1982, in Dallas.

Taylor, J. H., 1967, Two-dimensional brightness distributions of radio sources from Lunar occulation observations: Astrophys., **150**, 421–426.